Programmable Photonic Microwave Filters With Arbitrary Ultra-Wideband Phase Response

Shijun Xiao, *Member, IEEE*, and Andrew M. Weiner, *Fellow, IEEE*

***Abstract*—We present a coherent optical signal-processing approach for synthesis of programmable microwave phase filters over an ultra-wideband. Our scheme relies on a programmable optical phase filter implemented in a pulse-shaping geometry incorporating a spatial light modulator and hyperfine (∼600-MHz spectral resolution) optical spectral disperser. The user-defined optical phase filter is directly transferred to the electrical domain through heterodyne conversion, and the overall system response is characterized via vector network analyzer measurements. We illustrate our approach by synthesizing linear, quadratic, and cubic spectral phase functions over a 20-GHz band. To our best knowledge, this is the first realization of programmable arbitrary microwave phase filters over such a bandwidth.**

***Index Terms*—Microwave photonics, optical phase filters, photonic processing of microwave signals, pulse shaping.**

I. Introduction

PHOTONIC processing of microwave signals has been explored for nearly 30 years [1]–[4]. In general, microwave signals are imposed onto an optical carrier, manipulated directly in the optical domain, and then converted back into the microwave domain through opto-electronic (O/E) receivers [photodiodes (PDs)]. Compared to conventional electronic processing, advantages of photonic processing include ultra-wide bandwidth, immunity to electromagnetic interference, flexibility, etc., which bring attractive applications prospects in microwave and millimeter-wave engineering [5], [6]. Previous approaches have been referred to as discrete-time optical processing of microwave signals (DOPMS) [1], which can be modeled as tapped nonrecursive (finite impulse response) or recursive (infinite impulse response) digital filters. In order to avoid sensitivity to environmental conditions, the coherence time of the laser source is generally designed to be less than the tap delay, resulting in incoherent processing based on summation of powers. The main effort has been focused on realization of DOPMS architectures providing a specified amplitude filtering response, and previous results may be found in review papers [1], [7] and the references therein.

For more than two decades, approaches based on DOPMS have demonstrated a range of amplitude filters with desirable properties such as flat passbands, sharp transitions, and low sidelobes. Typically such filters exhibit linear phase response within passbands. However, little attention has been paid to engineering of the spectral phase response. One exception is photonic true time-delay generators, corresponding to adjustable linear phase response, which are of interest for beam steering in phased-array antenna systems [8]–[12]. However, to our best knowledge, there have been no reports on photonic microwave phase filters with user-defined nonlinear or arbitrary phase response. The ability to realize arbitrary broadband microwave phase filters could lead to new system concepts in ultra-wideband (UWB) systems [13]. Such systems include UWB wireless communications (3.1–10.6-GHz band), through-wall imaging and surveillance systems (1.99–10.6-GHz band), collision-avoidance radar (22–29-GHz band), and perhaps other applications not covered by Federal Communications Commission (FCC) regulation. Within the context of UWB systems, one important problem is that of antenna distortion [13]–[16]. Although a number of antenna designs with broadband amplitude response are available, such antennas often have an unfavorable nonlinear phase response resulting in dispersion. For pulsed excitation, this leads to strong signal distortions in the time domain, broadening the peak obtained at the receiving antenna and decreasing its amplitude. A microwave phase filter capable of being programmed for an appropriate nonlinear phase response could act as a matched filter to compensate such distortions, thereby optimizing receiver signal amplitudes, signal-to-noise ratio, and time resolution.

In this paper, we demonstrate programmable microwave phase filtering based on a novel coherent photonic processing scheme, which uses optical parallel filtering in the frequency domain in conjunction with optical heterodyne conversion, rather than the traditional tapped delay-line approach. The frequency-domain optical filtering is implemented using the well-known programmable optical pulse-shaping technique [17], which for the first time we have recently extended to hyperfine (∼600 MHz) spectral resolution [18]. In our system, the phase filter imposed onto the optical spectrum is directly mapped onto a microwave phase filter at the output. As a result, we have been able to demonstrate photonically implemented microwave phase filters that provide essentially arbitrary phase filter response over a microwave band from below 1 to 20 GHz with ∼600-MHz resolution under programmable control. Our spectral-domain pulse-shaping architecture provides fully coherent optical processing without significant sensitivity to environment conditions. Experiments on microwave phase filters with engineered families of linear phases, quadratic phases, and cubic phases are presented. Arbitrary microwave phase filtering is possible with our proposed approach. Comparable capability has not been previously reported to the best of our knowledge.

Manuscript received February 22, 2006; revised July 11, 2006.

The authors are with the School of Electrical and Computer Engineering, Purdue University, West Lafayette, IN 47907-2035 USA (e-mail: sxiao@ecn.purdue.edu; amw@ecn.purdue.edu).

Digital Object Identifier 10.1109/TMTT.2006.883237

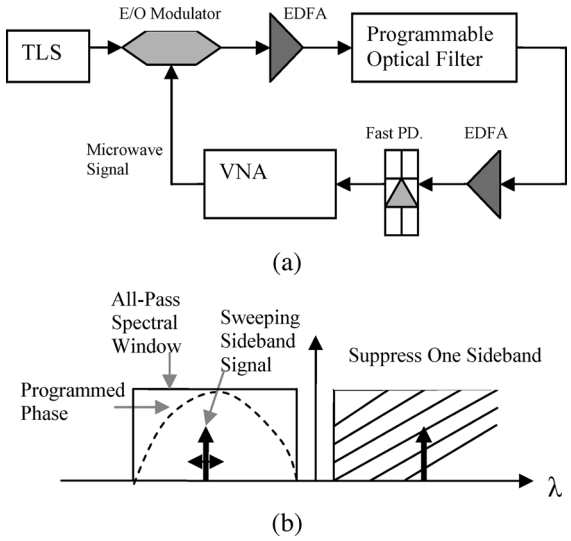

Fig. 1. (a) Experimental setup for photonic processing of microwave signals. TLS: tunable laser source. EDFA: erbium-doped fiber amplifier. VNA: vertical network analyzer. (b) Optical spectral sketch to illustrate the general principle of photonic processing.

We have recently demonstrated programmable UWB microwave amplitude filtering using a similar optical processing approach [18]. However, phase control was not discussed. In this paper, we report frequency-domain characterization of programmable phase responses using vector network analyzer (VNA) measurements. The application of such photonically implemented programmable phase filters for controlled time-domain reshaping of a pulsed (∼45 ps) electrical excitation is reported elsewhere [19].

The remainder of this paper is organized as follows. A theoretical analysis is presented in Section II. Section III introduces the experimental setup. Section IV discusses our experimental results on microwave phase filtering. We present a conclusion in Section V.

II. Theoretical Discussions

Fig. 1 shows our setup to implement coherent photonic processing of microwave signals via programmable hyperfine optical spectral filtering. A continuous wavelength (CW) optical carrier is passed through an MZM driven by an input microwave signal. Here we consider the case of input microwave signals that are single-frequency tones. This is appropriate for comparison to the swept-frequency measurements used in experiments. The modulator output field has a double-sideband format. Optical filtering suppresses one sideband while passing the carrier and the other sideband. Both amplitude and phase of the remaining sideband can be manipulated by the programmable hyperfine optical filter. The result is converted back to a microwave signal by heterodyne beating with the carrier on a fast PD.

If we assume that the microwave tone signal is applied to a single arm of the Mach–Zehnder modulator, the output optical field $E(t)$ can be described by

$$E(t) \propto \mathrm{Re}\left\{e^{j\omega_c t} + e^{j[\omega_c t+\delta+\pi A\cos(\Omega t)/V_\pi]}\right\} \tag{1}$$

where $\mathrm{Re}\{\}$ indicates the real part, ω_c is the optical carrier frequency, $\delta = \pi V_b/V_\pi$ is the phase shift caused by the dc bias V_b, V_π is the minimum transmission voltage parameter of the modulator, and $A\cos(\Omega t)$ is the input microwave tone signal. The first-order term in the Taylor series expansion of $E(t)$ in terms of $\pi A/V_\pi$ can be written as follows:

$$E(t) \propto \mathrm{Re}\left\{\left[e^{j\omega_c t} + e^{j(\omega_c t+\delta)}\right] + j\frac{\pi A}{2V_\pi}e^{j(\omega_c t+\Omega t+\delta)} + j\frac{\pi A}{2V_\pi}e^{j(\omega_c t-\Omega t+\delta)}\right\}. \tag{2}$$

This is valid for small-signal modulation ($\pi A/V_\pi \lesssim 0.1$).

Now we assume that an optical filter suppresses one sideband while modifying both the amplitude and phase of the remaining sideband. The result is

$$E(t) \propto \mathrm{Re}\left\{\left[e^{j\omega_c t} + e^{j(\omega_c t+\delta)}\right] + j\gamma(\omega_c+\Omega)\frac{\pi A}{2V_\pi}e^{j(\omega_c t+\Omega t+\delta)}e^{j\Phi(\omega_c+\Omega)}\right\} \tag{3}$$

where $\gamma(\omega_c+\Omega)$ represents the frequency-dependent amplitude transmission coefficient of the optical filter (γ is real, $0 \le \gamma(\omega_c+\Omega) \le 1$) and $\Phi(\omega_c+\Omega)$ represents its frequency-dependent phase response. In our treatment, we assume that the higher frequency (shorter wavelength) optical sideband is chosen. Note, however, that, in general, either one of the two sidebands can be chosen.

The PD current output is

$$i(t) \propto I(t) \propto \left\langle E^2(t)\right\rangle_{\omega_c} \propto 2\cos^2(\delta/2) + \frac{1}{2}\left[\gamma_m(\Omega)\frac{\pi A}{2V_\pi}\right]^2 - \cos(\delta/2)\gamma_m(\Omega)\frac{\pi A}{V_\pi}\sin\left[\Omega t + \Phi_m(\Omega) + \delta/2\right] \tag{4}$$

where $i(t)$ is the PD current and $I(t)$ is the optical intensity averaged over the oscillations of the optical carrier. Please note that we assume a linear PD: the current is proportional to the input light intensity. For simplicity, we have introduced the notation $\gamma_m(\Omega) = \gamma(\omega_c+\Omega)$ and $\Phi_m(\Omega) = \Phi(\omega_c+\Omega)$. The voltage signal consists of a dc component, as well as a filtered ac signal. For the ac signal, this represents a filter with spectral amplitude response $\gamma_m(\Omega)$, as well as spectral phase response $\Phi_m(\Omega)$.

The frequency-dependent microwave signal delay τ is calculated by

$$\tau(\Omega) = -\frac{d\Phi_m(\Omega)}{d\Omega}. \tag{5}$$

According to (5), true time delay can be obtained by programming the optical filter for linear spectral phase, while programmable frequency-dependent delay functions can be obtained by setting the optical filter for quadratic or higher order spectral phase. According to (4), a simultaneous amplitude filtering window may also be obtained simultaneously with user-defined phase filtering. With both amplitude and phase filtering, our approach should provide unprecedented capabilities to control microwave signals over an UWB.

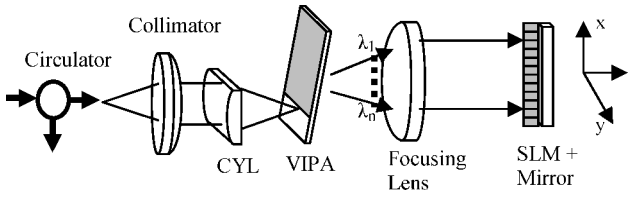

Fig. 2. Experimental setup of our programmable coherent optical filter based on a VIPA. CYL: cylindrical lens. SLM: spatial light modulator.

III. Experimental Setup

Our general experimental setup, sketched in Fig. 1, is similar to that discussed in [18]. For completeness, however, we provide a description in the following. A tunable laser with linewidth below 0.1 pm (∼12.5 MHz) is input into a Mach–Zehnder intensity modulator (MZM) with an electrical −3-dB passband >30 GHz, which is used to impose a microwave modulation signal onto the optical carrier. The modulator has a single electrode input and a minimum transmission voltage $V_\pi \sim 5.0$ V. The input microwave tone from a network analyzer is swept from 0.05 to 20.05 GHz (instrumental limit) at a step of 0.05 GHz with a constant RF power level at −5 dBm corresponding to an amplitude voltage of 0.18 V for 50-Ω impedance ($\pi A/V_\pi = 0.11$). The modulator is biased for double-sideband modulation with partial carrier suppression in order to yield approximately equal carrier and sideband amplitudes, i.e., $|\cos(\delta/2)| \approx \pi A/V_\pi$. This maximizes the RF signal gain in the case where the optical path includes a saturated amplifier with slow saturation dynamics, as for erbium-doped fiber amplifiers (EDFAs) [18]. After amplification in an EDFA, the signal passes through the programmable optical filter (discussed below). The optical filter suppresses one of the optical sidebands (suppression ratio >25 dB) while imposing the desired phase response (and amplitude response when desired) onto the remaining sideband. After a second optical amplifier, the optical signal is directed onto a fast PD, which has an electrical −3-dB bandwidth of ∼60 GHz. The resultant microwave signal is measured by the VNA.

Fig. 2 is the setup of our programmable optical filter. As in traditional pulse shaping [17], different optical frequency components contained within the input signal are first separated spatially using a spectral disperser and lens combination, and then a spatial light modulator (SLM) manipulates the phase and/or amplitude of the different frequency components in parallel. Here, the optical filter is implemented using a reflective geometry pulse shaper, and a virtually imaged phased array (VIPA) [20] rather than the usual diffraction grating is used as the optical spectral disperser. In our implementation, the VIPA has a free spectral range of 50 GHz (0.4 nm) at 1.55-μm wavelength. The input optical frequency components are dispersed by the VIPA and collimated by a cylindrical lens with a focal length of 300 mm. A commercial liquid-crystal programmable SLM is placed at the back focal plane of the lens. The SLM is constructed of two liquid-crystal layers, each of which has 128 individually addressable pixels arranged along a line with pixel-to-pixel spacing of 100 μm. By using a polarizer at the output, this allows simultaneous and independent gray-level amplitude and phase filtering of individual optical frequency components [21]. The spectral resolution in our setup is ∼600 MHz. A flat mirror very close to the SLM reflects the light that then double passes through the SLM. Reprogramming speed is dictated by the SLM response, which is on the order of tens of milliseconds scalable down to perhaps milliseconds for the liquid-crystal displays commonly used in pulse shaping [17].

There are two principal factors limiting the spectral resolution in our current experiments. First, each pixel of the SLM corresponds to approximately 600 MHz of optical frequency spread. By choosing a larger focal length lens, the frequencies can be further dispersed. Since we are currently using only ∼30 pixels out of our 128 pixel SLM, a factor of four improvement should be possible. Second, the finite optical spot size at the SLM also fundamentally limits spectral resolution [17]. With our current VIPAs, this limit is also approximately 600 MHz. This spectral resolution limit is a property of the specific spectral dispersing device used and is not improved simply by increasing the focal length [22]. The fundamental spectral resolution of our VIPA shaper can be further improved in proportion to decreases in the VIPA FSR, but reducing the FSR also limits the processing bandwidth of microwave signals.

We have previously published several papers demonstrating the application of VIPAs for high spectral resolution optical signal processing and sensing [23]–[25]. There have also been a few previous reports of VIPAs incorporated into reflective geometry pulse shapers for optical phase filtering. A VIPA-based pulse shaper that used a curved mirror (rather than a programmable SLM) for dispersion compensation in optical fiber transmission was reported in [26] and [27]. Another group reported a VIPA-based pulse shaper with fixed spatial phase masks and 5-GHz spectral resolution for optical code-division multiple-access phase encoding [28]. Our group recently has reported the first implementation of an electronically programmable VIPA-based pulse shaper incorporating a liquid-crystal SLM [29]. In that study, the VIPA had a free spectral range of 400 GHz, and spectral resolution was on the order of a few tens of gigahertz. In this paper, we demonstrate the first high spectral resolution VIPA-based pulse shaper configured for programmable spectral phase control, as well as the first application to wideband microwave phase filtering. The high spectral resolution achieved in the current experiments is crucial for the microwave phase-filtering application.

IV. Microwave Spectral Phase Filtering

According to our theoretical analysis, programmable optical phase filtering can be directly mapped to the microwave domain via heterodyne conversion. This results in a microwave phase-filtering functionality that can be measured through the VNA. Various microwave spectral phase-filtering results are presented here to illustrate the capability of our approach. As our VNA has a bandwidth limited from dc to 20 GHz, we only make use of a group of 31 SLM pixels that match this 20-GHz bandwidth.

In Figs. 3 and 4, we present data for which the SLM is programmed to ideally provide pure spectral phase filtering, i.e., ideally there is no intended attenuation of the amplitude. Fig. 3(a) shows a set of linear spectral phase-filtering results, where both positive and negative phase slopes are shown. We program linear phase profiles characterized by

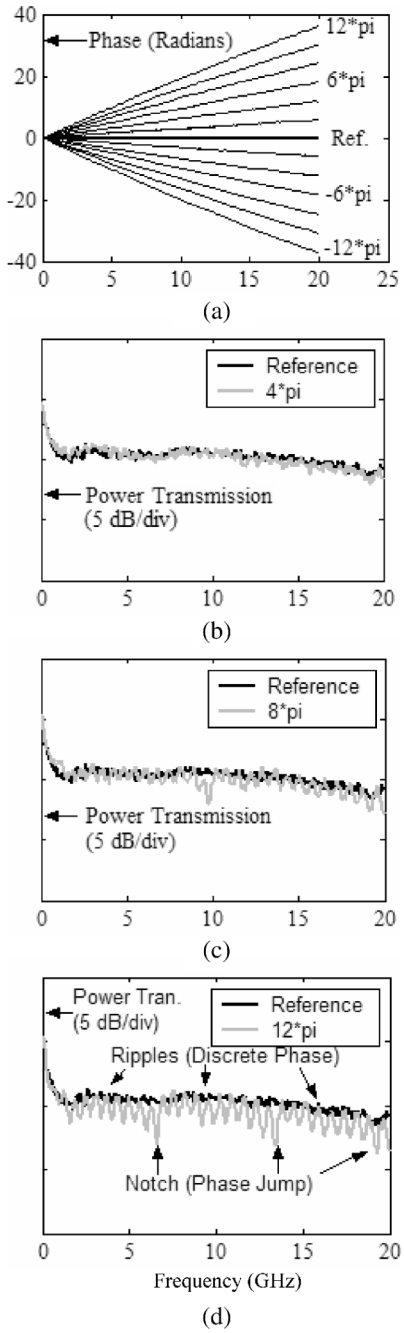

Fig. 3. (a) Programmed microwave linear spectral phase filtering. (b)–(d) Power transmission for three linear phases with the different slopes, respectively, and the reference is without phase programming.

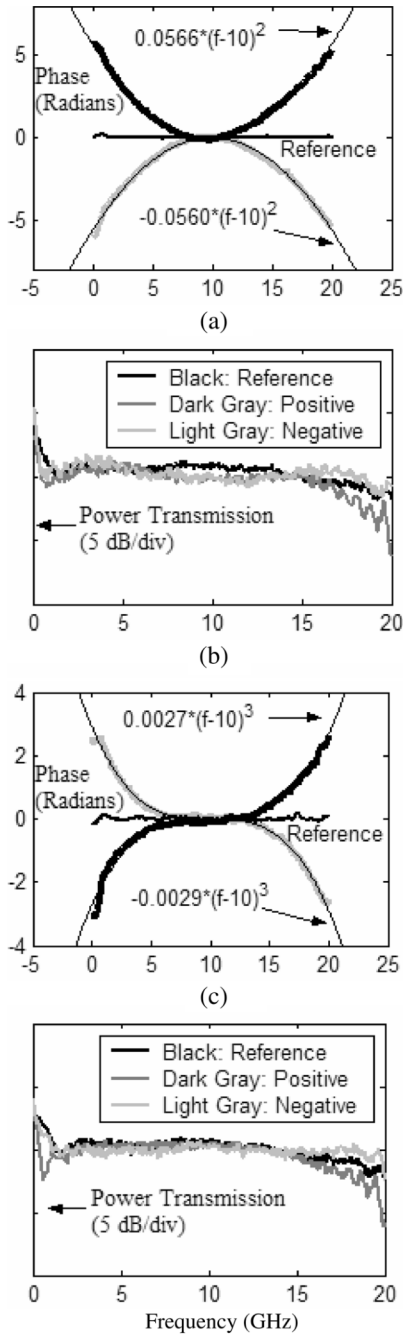

Fig. 4. (a) and (b) Programmed microwave quadratic spectral phase filtering and power transmission, respectively. (c) and (d) Programmed microwave cubic spectral phase and power transmission, respectively. The reference is without phase programming. Thick lines in (a) and (c) indicate experimental data, and thin lines indicate curve fitting.

$\Phi(N) = (N-60)/30 * m\pi$ across pixels #45–#75, where N is the pixel number and m is an integer. Here, higher microwave frequencies correspond to smaller pixel numbers, and vice versa. The horizontal line is the reference, for the case of no phase programming ($m = 0$), with a constant linear phase subtracted (corresponding to the delay bias in our setup). The slope varies from $-12\pi/20$ GHz ($m = 12$) to $12\pi/20$ GHz ($m = -12$) at a step of $2\pi/20$ GHz. The maximum slope is $12\pi/20$ GHz, indicating a time delay of -300 ps, and the minimum slope is $-12\pi/20$ GHz, indicating a time delay of 300 ps.

Fig. 3(b)–(d) shows examples of the power response measured by the VNA. The minimum microwave power insertion loss is $\sim$8 dB at mid-passband for filters implemented in our current setup. Three positive slope cases ($4\pi/20$ GHz, $8\pi/20$ GHz, and $12\pi/20$ GHz) are plotted, in each case together with a reference curve corresponding to the power response with the SLM programmed for constant phase. The negative slope cases (not shown) are similar. For the case of 4π, total phase variation, the power response is very close to the reference. However, for

larger total phase variations, notches appear in the power response.

The origin of the notches is explained through the following discussion. Since the liquid-crystal SLM has a limited continuously programmable phase range, we need to apply a wrapped phase profile when the range of the targeted phase profile exceeds the SLM's phase range. Four our double-pass pulse-shaping geometry, we limit the applied phase range to 4π; for larger phase excursions, we apply the target phase modulo 4π. This leads to phase jumps of 4π at certain pixel locations. Although ideally phase jumps of 4π in double pass (2π in single pass) should have no effect, in practice, effects that may arise from discontinuities in the liquid-crystal orientations lead to notches at the locations of the 4π phase jumps. In addition, smaller phase jumps resulting from the discrete (pixilated) nature of the phase programmed onto the SLM cause additional amplitude notches. These additional notches become larger for increasing phase change per pixel and are most obvious ($\sim$1.5-dB power fluctuation) in Fig. 3(d) where the phase change per pixel is 0.4π. These additional notches arise from the finite size of individual focused optical frequency components at the SLM plane, which results in an optical filtering function that is a smeared version of the SLM pattern. This fundamentally leads to a phase-to-amplitude conversion process that is well understood in the pulse-shaping literature [17], [30]. In general, such phase-to-amplitude conversion processes provide a limit on the delay range (with small-signal distortions) obtainable via our approach. In any case, we have shown nearly continuously programmable linear phase-filtering functions that may generate user-defined true time delay up to 600 ps over a 20-GHz band with power ripples limited to a few decibels. We have recently published time-domain experiments confirming the ability to generate true programmable time delays for short electrical pulses [19]. In these experiments, we demonstrated a delay range up to 710 ps for an input electrical pulse with a duration $\sim$45 ps. The energy loss at the largest delay range is approximately 50%, where the pulse's duration is broadened to $\sim$75 ps.

The control of time delay via spectral phase pulse shaping has been performed previously within the context of ultrafast optics [17]. In the case of grating-based pulse shapers, the resulting time changes are understood to arise physically due to beam deflection caused by the spatial phase gradient programmed onto the SLM, leading to changes in the beam trajectory and optical path length through the apparatus. In the case of VIPA-based pulse shapers, the physical explanation for the achieved time delay changes still involves beam deflection by the SLM spatial phase function, but is modified: deflection causes the return beam to reenter the VIPA at a slightly displaced location, leading to a change in the number of bounces the beam must execute while it is trapped in the VIPA before it exits at the antireflection coated window. For both grating- and VIPA-based pulse shapers, the maximum achievable time delay is roughly equal to the inverse of the available spectral resolution. For larger time delays, the beam deflection exceeds the beam size, leading to significant energy loss. Furthermore, both pulse advancement and retardation are possible, again within spectral resolution limits. Due to the large fixed delay of the overall setup, programmable pulse advancement can be achieved without violating causality. This discussion is general and applies equally to linear spectral phase (true-time delay) and quadratic and cubic spectral phase, as well as other cases not explicitly shown here.

It is worth comparing our method with the acoustic-optic frequency-dependent phase compensation (AO-FDPC) technique [11], [12] that has previously been investigated for microwave time-delay generation. In AO-FDPC, optical spectral dispersion is generated as part of the microwave to optical transduction process. The time delay fundamentally arises from the slow acoustic wave propagation velocity in the acoustic-optic (AO) crystal, and programmability is achieved essentially by optically selecting which portion of the AO active area is imaged onto the PD. In our method the optical spectral dispersion process and the microwave to optical transduction process are separated. Furthermore, the time-delay mechanism is fundamentally optical in nature and may be described directly as a Fourier synthesis process, which applies both to true-time delays, as well as more general waveform shaping operations. In terms of the conditions outlined in [11], the time delay and the signal bandwidth cannot exceed the storage time and the operating bandwidth, respectively, of the processing system. Similar conditions are well known in the optical pulse-shaping literature [17]. In the current experiments, the optical beam bounces back and forth over 50 times in the VIPA spectral disperser, corresponding to a delay of order 1 ns (etalon $\sim$1.5 mm, refractive index $\sim$2). The VIPA has a bandwidth (free spectral range) of 50 GHz. The input electrical impulses in our time-domain experiments reported in [19] have a duration $\sim$ 45 ps $\ll$ 1 ns and a bandwidth $\sim$ 30 GHz $<$ 50 GHz, which satisfy the requirements discussed in [11].

Fig. 4 illustrates some examples of nonlinear spectral phase filtering. Fig. 4(a) and (b) shows two examples of quadratic spectral phase filtering together with the corresponding power transmission spectra. Here we program quadratic phase profile $\Phi(N) = (N-60)^2/30^2 * m\pi$ ($m = 2$ or -2) across pixels #45–#75. Opposite signs are shown in black ($m = 2$) and gray ($m = -2$) solid lines. The phase plot is referenced to the case of no phase programming (approximately horizontal line in plot) after subtracting a constant linear phase. In addition, numerical fits are plotted together with the VNA data to illustrate the quadratic variation. Fig. 4(c) and (d) is examples of cubic spectral phase filtering and the corresponding power transmission spectra. Here we program cubic phase profiles $\Phi(N) = (N-60)^3/30^3 * m\pi$ ($m = 1$ or -1) across pixels #45–#75. Opposite signs are shown in black ($m = 1$) and gray ($m = -1$) solid lines. Numerical cubic fits are also plotted to illustrate cubic variation. Comparing to the reference, the power transmission for the quadratic and cubic phase examples as only relatively small deviations ($<\sim$1-dB power variations) over the full bandwidth, except at the cutoffs at dc and 20 GHz. The relatively large deviations at these cutoffs may be partially suppressed by carefully extending the phase programming by a few pixels more beyond the used pixel number range #45–#75.

Fig. 5 includes some examples of nonlinear spectral phase filtering together with amplitude filtering with potential applications in UWB (3.1–10.6 GHz) systems [11]. Compared to Fig. 4, we program an amplitude response that constitutes a

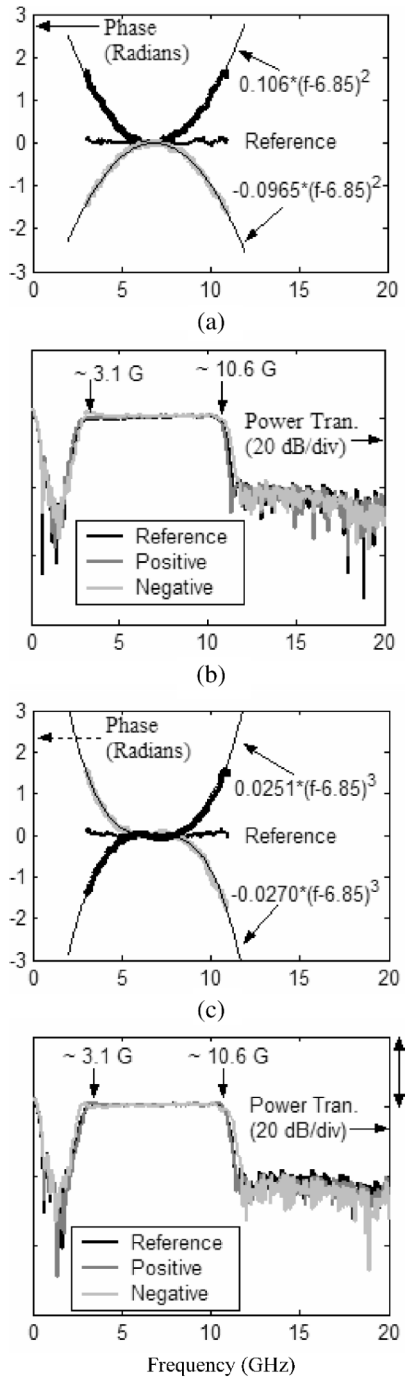

Fig. 5. Programmed microwave quadratic and cubic spectral phase filtering UWB (3.1–10.6 GHz) applications: (a) quadratic spectral phase filtering in (b) an UWB window; (c) cubic spectral phase filtering in (d) an UWB window. Thick lines in (a) and (c) indicate experimental data and thin lines indicate curve fitting.

bandpass filter for the specified UWB band, while simultaneously applying either quadratic or cubic spectral phase within the passband. The plots are organized in a similar way as in Fig. 4. In addition to the desired phase response, we are able to simultaneously generate bandpass filters with passband variations of ∼1 dB in power. This illustrates the high degree of flexibility in microwave filter synthesis enabled by our photonic processing technique.

V. Conclusion

We have demonstrated a photonic processing method for programmable microwave phase filtering, which allows generation of arbitrary phase filters over an ultrawide bandwidth. The current experiments demonstrate realization of user-defined phase filters over a range from ∼600 MHz to 20 GHz (limited by our test instrumentation) with a resolution of ∼600 MHz. Our approach exploits programmable hyperfine optical phase filtering in the 1.55-μm lightwave band, followed by heterodyne conversion to the electrical domain. We have presented a theoretical analysis and reported several experimental examples. We have demonstrated programmable linear phase filtering over the 20-GHz band with potential application to true time delay for phased-array antenna systems; we also demonstrated programmable synthesis of nonlinear (quadratic and cubic) spectral phase, which may be useful for compensation of phase distortions in pulse-excited broadband antennas. Finally, we have demonstrated simultaneous programmable amplitude and phase filtering.

Acknowledgment

The authors would like to thank C. Lin, Avanex Corporation, Fremont, CA, for providing VIPA devices. The authors also like to thank both Prof. D. Peroulis and Prof. W. J. Chappell, both with Purdue University, West Lafayette, IN, for loaning the VNA.

References

[1] J. Capmany, B. Ortega, D. Pastor, and S. Sales, "Discrete-time optical processing of microwave signals," *J. Lightw. Technol.*, vol. 23, no. 2, pp. 702–723, Feb. 2005.

[2] C. Chang, J. A. Cassaboom, and H. F. Taylor, "Fiber optical delay line devices for RF signal processing," *Electron. Lett.*, vol. 13, pp. 678–680, 1977.

[3] K. Jackson, S. Newton, B. Moslehi, M. Tur, C. Cutler, J. Goodman, and H. J. Shaw, "Optical fiber delay-line signal processing," *IEEE Trans. Microw. Theory Tech.*, vol. MTT-33, no. 3, pp. 193–210, Mar. 1985.

[4] D. E. N. Davies and G. W. James, "Fiber and integrated optical devices for signal processing," *Electron. Lett.*, vol. 20, pp. 95–96, 1984.

[5] R. A. Minasian, K. E. Alameh, and E. H. W. Chan, "Photonics-based interference mitigation filters," *IEEE Trans. Microw. Theory Tech.*, vol. 49, no. 10, pp. 1894–1899, Oct. 2001.

[6] D. Pastor, B. Ortega, J. Capmany, P.-Y. Fonjallaz, and M. Popov, "Tunable microwave photonic filter for noise and interference suppression in UMTS base stations," *Electron. Lett.*, vol. 40, no. 16, pp. 997–999, Aug. 2004.

[7] J. Capmany, D. Pastor, B. Ortega, J. Mora, and M. André, "Photonic processing of microwave signals," *Proc. Inst. Elect. Eng.—Optoelectron.*, vol. 152, no. 6, pp. 299–320, Dec. 2005.

[8] W. Ng *et al.*, "The first demonstration of an optically steered microwave phased array antenna using true-time-delay," *J. Lightw. Technol.*, vol. 9, no. 9, pp. 1124–1131, Sep. 1991.

[9] B. Ortega, J. L. Cruz, J. Capmany, M. V. Andres, and D. Pastor, "Variable delay line for phased-antenna based on a chirped fiber grating," *IEEE Trans. Microw. Theory Tech.*, vol. 48, no. 8, pp. 1352–1360, Aug. 2000.

[10] Y. Liu, J. Yang, and J. Yao, "Continuous true-time-delay beamforming for phased array antenna using a tunable chirped fiber grating delay line," *IEEE Photon. Technol. Lett.*, vol. 14, no. 8, pp. 1172–1174, Aug. 2002.

[11] W. D. Jemison, "Analysis of the AO-FDPC optical heterodyne technique for microwave time delay and phased array beamsteering applications," *IEEE Trans. Microw. Theory Tech.*, vol. 50, no. 7, pp. 1832–1843, Jul. 2002.

[12] E. N. Toughlian and H. Zmuda, "A photonic variable RF delay line for phased array antennas," *J. Lightw. Technol.*, vol. 8, pp. 1824–1828, Dec. 1990.
[13] J. H. Reed, Ed., *An Introduction to Ultra Wideband Communication Systems*. Upper Saddle River, NJ: Prentice-Hall, 2005.
[14] A. Shlivinski, E. Heyman, and R. Kastner, "Antenna characterization in the time domain," *IEEE Trans. Antennas Propag.*, vol. 45, no. 7, pp. 1140–1149, Jul. 1997.
[15] D. M. Pozar, "Waveform optimizations for ultrawideband radio systems," *IEEE Trans. Antennas Propag.*, vol. 51, no. 9, pp. 2335–2345, Sep. 2003.
[16] J. D. McKinney and A. M. Weiner, "Compensation of the effects of antenna dispersion on UWB waveforms via optical pulse shaping techniques," *IEEE Trans. Microw. Theory Tech.*, vol. 54, no. 4, pp. 1681–1686, Apr. 2006.
[17] A. M. Weiner, "Femtosecond pulse shaping using spatial light modulators," *Rev. Sci. Instrum.*, vol. 71, no. 5, pp. 1929–1960, May 2000.
[18] S. Xiao and A. M. Weiner, "Coherent photonic processing of microwave signals using spatial light modulator: Programmable amplitude filters," *J. Lightw. Technol.*, vol. 24, no. 7, pp. 2523–2529, Jul. 2006.
[19] ——, "Coherent Fourier transform electrical pulse shaping," *Opt. Express*, vol. 14, no. 7, pp. 3073–3082, Apr. 2006.
[20] M. Shirasaki, "Large angular dispersion by a virtually imaged phased array and its application to a wavelength demultiplexer," *Opt. Lett.*, vol. 21, no. 5, pp. 366–368, Mar. 1996.
[21] M. M. Wefers and K. A. Nelson, "Generation of high-fidelity programmable ultrafast optical waveforms," *Opt. Lett.*, vol. 20, no. 9, pp. 1047–1049, May 1995.
[22] S. Xiao and A. M. Weiner, "Experimental and theoretical study of hyperfine WDM demultiplexer performance using the virtually imaged phased-array," *J. Lightw. Technol.*, vol. 23, no. 3, pp. 1456–1467, Mar. 2005.
[23] ——, "Optical carrier suppressed single sideband (O-CS-SSB) modulation using a hyperfine blocking filter based on a virtually-imaged phased-array (VIPA)," *IEEE Photon. Technol. Lett.*, vol. 17, no. 7, pp. 1522–1524, Jul. 2005.
[24] ——, "4-user, ~3 GHz-spaced sub-carrier multiplexing (SCM) using optical direct-detection via hyperfine WDM," *IEEE Photon. Technol. Lett.*, vol. 17, no. 10, pp. 2218–2220, Oct. 2005.
[25] S. X. Wang, S. Xiao, and A. M. Weiner, "Broadband, high spectral resolution 2-D wavelength-parallel polarimeter for dense WDM systems," *Opt. Express*, vol. 13, no. 23, pp. 9374–9380, Nov. 2005.
[26] M. Shirasaki, "Chromatic-dispersion compensator using virtually imaged phased array," *IEEE Photon. Technol. Lett.*, vol. 9, no. 12, pp. 1598–1561, Dec. 1997.
[27] H. Ooi, K. Nakamura, Y. Akiyama, T. Takahara, T. Terahara, Y. Kawahata, H. Isono, and G. Ishikawa, "40-Gbps WDM transmission with virtually imaged phased array (VIPA) variable dispersion compensators," *IEEE J. Lightw. Technol.*, vol. 20, no. 12, pp. 2196–2203, Dec. 2002.
[28] S. Etemad, P. Toliver, R. Menendez, J. Young, T. Banwell, S. Galli, J. Jackel, P. Delfyett, C. Price, and T. Turpin, "Spectrally efficient optical CDMA using coherent phase-frequency coding," *IEEE Photon. Technol. Lett.*, vol. 17, no. 4, pp. 929–931, Apr. 2005.
[29] G. Lee and A. M. Weiner, "Programmable optical pulse burst manipulation using a virtually imaged phased array (VIPA) based Fourier transform pulse shaper," *J. Lightw. Technol.*, vol. 23, no. 11, pp. 3916–3923, Nov. 2005.
[30] R. N. Thurston, J. P. Heritage, A. M. Weiner, and W. J. Tomlinson, "Analysis of picosecond pulse shape synthesis by spectral masking in a grating pulse compressor," *IEEE J. Quantum Electron.*, vol. QE-22, no. 5, pp. 682–696, May 1986.

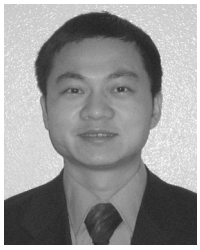

Shijun Xiao (S'03–M'05) was born in Chengdu, China, in 1979. He received the B.S. degree in electronics from Beijing University, Beijing, China, in 2001, and the M.S. and Ph.D. degrees in electrical and computer engineering from Purdue University, West Lafayette, IN, in 2003 and in 2005, respectively.

He is currently a Postdoctoral Research Associate with the School of Electrical and Computer Engineering, Purdue University. He has authored or coauthored nearly 30 journal and conference papers. His research interests include optical signal processing, optical pulse shaping, optical fiber communications, microwave photonics, micrometer/nanometer-scale photonics. He has been a reviewer for *Optics Communications*.

Dr. Xiao is a member of the IEEE Lasers and Electro-Optics Society and the Optical Society of America (OSA). He has served as a reviewer for the JOURNAL OF LIGHTWAVE TECHNOLOGY. He was the recipient of the Andrews Fellowship presented by Purdue University (2001–2003) and the IEEE LEOS Graduate Student Fellowship (2004). He was a finalist for the Dimitris N. Chorafas Foundation Award of Purdue University (2005).

Andrew M. Weiner (S'84–M'84–SM'91–F'95) received the Sc.D. degree in electrical engineering from the Massachusetts Institute of Technology (MIT), Cambridge, in 1984.

From 1979 to 1984, he was a Fannie and John Hertz Foundation Graduate Fellow with MIT. Upon graduation, he joined Bellcore, initially as a Member of Technical Staff and then as Manager of Ultrafast Optics and Optical Signal Processing Research. In 1992, he joined Purdue University, West Lafayette, IN, where he is currently the Scifres Distinguished Professor of Electrical and Computer Engineering. From 1997 to 2003 he was the Electrical and Computer Engineering Director of Graduate Admissions. He has authored five book chapters, over 160 journal papers, and coedited one book. He has also authored or coauthored over 300 conference papers, including approximately 80 conference invited talks. He has presented over 70 additional invited seminars at university, industry, and government organizations. He holds eight U.S. patents. His research focuses on ultrafast optical signal processing and high-speed optical communications. He is especially well known for pioneering the field of femtosecond pulse shaping, which enables generation of nearly arbitrary ultrafast optical waveforms according to user specification. He has served as an Associate Editor for *Optics Letters*.

Prof. Weiner is a Fellow of the Optical Society of America. He has served on or chaired numerous research review panels, professional society award committees, and conference program committees. From 1988 to 1989, he served as an IEEE Lasers and Electro-Optics Society (IEEE LEOS) Distinguished Lecturer. He has served as chair or co-chair of the Conference on Lasers and Electro-Optics, the Gordon Conference on Nonlinear Optics and Lasers, and the International Conference on Ultrafast Phenomena. He has also served as associate editor for the IEEE JOURNAL ON QUANTUM ELECTRONICS and the IEEE PHOTONICS TECHNOLOGY LETTERS. Prof. Weiner served as an elected member of the Board of Governors of the IEEE LEOS (1997–1999) and as secretary/treasurer of IEEE LEOS (2000–2002). From 2002 to 2005, he was a vice-president (representing IEEE LEOS) of the International Commission on Optics (ICO). He has been the recipient of numerous awards including the Hertz Foundation Doctoral Thesis Prize (1984), the Adolph Lomb Medal of the Optical Society of America (1990), the Curtis McGraw Research Award of the American Society of Engineering Education (1997), the International Commission on Optics Prize (1997), the IEEE LEOS William Streifer Scientific Achievement Award (1999), the Alexander von Humboldt Foundation Research Award for Senior U.S. Scientists (2000), and the inaugural Research Excellence Award from the Schools of Engineering at Purdue (2003).